Electronic Supplementary Material (ESI) for ChemComm.

Capture the Transient Species at the Electrode-Electrolyte Interface by In Situ Dynamic Molecular Imaging

Jiachao Yu,[ab‡] Yufan Zhou,[c‡] Xin Hua,[ab] Songqin Liu,[*a] Zihua Zhu,[*c] and Xiao-Ying Yu[*b]

[a]Jiangsu Province Hi-Tech Key Laboratory for Bio-medical Research, School of Chemistry and Chemical Engineering, Southeast University, Nanjing 210096, China. E-mail: liusq@seu.edu.cn, Tel: (+86) 138-5152-1532
[b]Earth and Biological Sciences Directorate, Pacific Northwest National Laboratory, Richland, WA 99354, USA. E-mail: xiaoying.yu@pnnl.gov, Tel: (+1) 509-372-4524
[c]Environmental Molecular Sciences Laboratory, Pacific Northwest National Laboratory, Richland, WA 99354, USA. E-mail: zihua.zhu@pnnl.gov, Tel: (+1) 509-371-6240
[‡] Equal contribution

EXPERIMENTAL DETAILS

Our in situ electrochemical device incorporated three electrodes including a gold working electrode (WE), platinum counter electrode (CE), and platinum pseudo reference electrode (RE). The electrochemical system was encapsulated in PDMS using soft lithography technology.[1, 2] The gold WE film (30 nm thick, 2 × 2 mm^2 in area) was sputter coated on the silicon nitride (SiN) membrane window (100 nm thick, 0.5×0.5 mm^2) on a silicon frame (200 μm thick, 7.5×7.5 mm^2, Norcada Inc., Canada). A narrow strip of gold extended from the gold WE to the edge of the silicon frame was connected to a silver wire (0.25 mm outside diameter OD, Sigma Aldrich). An electrochemical workstation was used to apply potentials to the device. Two Pt wires (0.25 mm OD) were embedded in the PDMS block, one end (3 mm in length) exposed in the microchannel as CE or RE, the other end (10 mm in length) exposed outside the PDMS block for connecting with the external circuit of electrochemical workstation.

Two metal tubings (0.5" long) were bent to 90° and inserted into the two punched holes in PDMS. The other ends of the metal tubings were inserted into two PTFE tubings (Sigma Aldrich, St. Louis, MI, USA). The PDMS piece with CE/RE and the WE silicon frame were treated with oxygen plasma (March Plasma Systems, Concord, CA), aligned, and irreversibly bonded. The bonded assembly was then encapsulated into PDMS for sealing. The PDMS block was finally cut to size.

Aqueous solutions of 10 mM potassium iodide (Aldrich, 99.9%) were prepared using ultrapure water (Milli-Q Integral Water Purification System, EMD Millipore, Billerica, MA, USA). Solutions were filled into the system through one end of the PTFE tubing (OD 1/16 inch, Vici) by a syringe pump (Harvard apparatus, Holliston, Massachusetts). After filling the electrolyte solution, two PTFE tubings were connected with a union and fittings (Upchurch, Oak Harbor, WA, USA).

The vacuum compatible electrochemical device was mounted on the ToF-SIMS heating stage and deployed in a ToF-SIMS 5 instrument (IONTOF GmbH, Münster, Germany). ToF-SIMS rasters a pulsed focused primary ion beam over the sample. Ejected secondary ions are separated by a time-of-flight mass analyzer to form surface chemical maps. The ToF-SIMS provides molecular information on the top nm of the liquid. The aperture size (*e.g.*, ~2 μm in this study) is large enough to permit the analytical methods like ToF-SIMS to cleanly probe within the aperture, yet small enough to limit mean-free path issues and fluid loss.[2] Evaporating vapor is dense only around the distance of the aperture diameter away from the device. A 25 keV Bi_3^+ beam was used as the primary ion beam in this study, while the energy of secondary ions typically ranges from 0 to 10 eV. The Bi_3^+ beam current was ~1.0 pA with a pulse width of 150 ns and a cycle time of 100 μs. The Bi_3^+ beam was focused to about 0.4 μm in diameter and it was rastered in the circular area of the aperture with ~2 μm diameter. After the SiN and Au electrode membrane were punched through (indicated by the sudden intensity change of OH^- and SiN^-), the same condition was maintained for a sufficient period of time to collect real-time electrochemical ToF-SIMS data. The main chamber operating vacuum pressure during measurements was ~5×10^{-7} mbar.

The electrochemistry was initiated right before the starting the Bi_3^+ primary ion beam. Current-time curve and cyclic voltammetry were used in this study by an electrochemical workstation

(660A Electrochemical Workstation, CH Instruments, Inc., Austin, TX, USA). For current-time curve mode, 0 V, 0.4 V and 1 V were applied on the working electrode respectively. For cyclic voltammetry mode, the potential initiated from 0 V and then scanning between 0 V to 1 V at a scan rate of 20 mV/s. After the ToF-SIMS measurement was ended, the electrochemistry was stopped.

The SIMS data were mass calibrated using CH^-, OH^-, C_2H^-, C_3H^-, I^- and Au^- peaks. Specific peaks (*i.e.*, OH^-, SiN^-, I^-, I_2^-, I_3^-, IO^-, IO_2^-, IO_3^-, AuI^-, AuI_2^- and Au_2I^-) were selected for data analysis. The reduction of raw data and the reconstruction of 3D images were performed using the SurfaceLab 6 software (IONTOF, Germany).

SUPPLEMENTARY FIGURES

Fig. S1 depicts a schematic drawing show the diffusion of intermediates and products in and around the hole on the SiN membrane. The thickness of SiN membrane is 100 nm and the thickness of Au thin film is 30 nm. The hole size is ~2 μm in diameter. The dimension in the cartoon is exaggerated to illustrate the concept but not exactly proportional to the length scale.

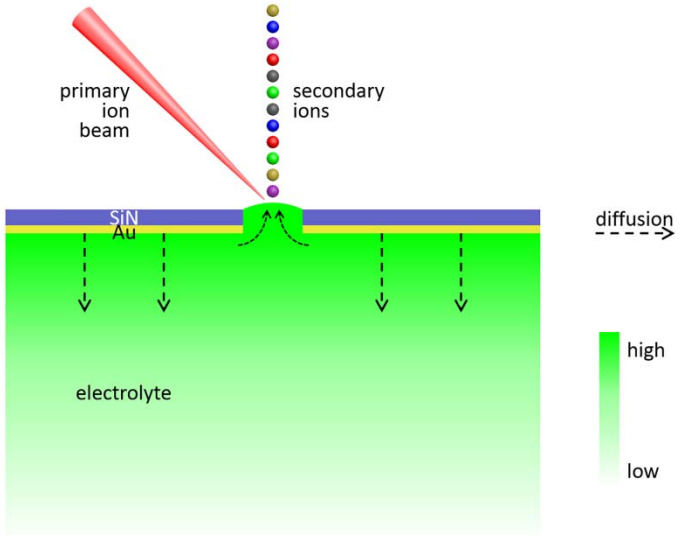

Fig. S1 Schematic of the diffused intermediate species and products in and around the ~2 μm hole. The green color legend showed the concentration gradient of intermediate species and products. Darker color indicates higher concentration and lighter color lower concentration. The primary ion beam is depicted in red. The secondary ions generated at the liquid surface being extracted to the time-of-flight mass analyzer are shown in color spheres.

There is more detailed discussion in our earlier publication quoted as the following:[3]

"Normally, the information depth for static ToF-SIMS is estimated to be a few nm according to reported SIMS emission depth measurements. However, the interface is very dynamic in this work. As described in Fig. S-2, a high ion dose was used (*i.e.*, $>4\times10^{16}$ ions cm^{-2}), and SiN/Au erosion occurred continuously. In a liquid system, ion species of interest may diffuse from the adjacent electrode/electrolyte interface or the bulk to the aperture area (*e.g.*, 10^{-9}-10^{-6} m). Furthermore, the aqueous solution surface is self-renewable due to liquid flow and evaporation. Therefore, the SIMS spectra shown here contain information not only from the electrode/electrolyte interface (a few nm thick), but also from the electrolyte liquid (up to a few microns) and the aperture side wall (SiN/Au)."

Fig. S2 shows one cycle of the cyclic voltammetry in Fig. 3.

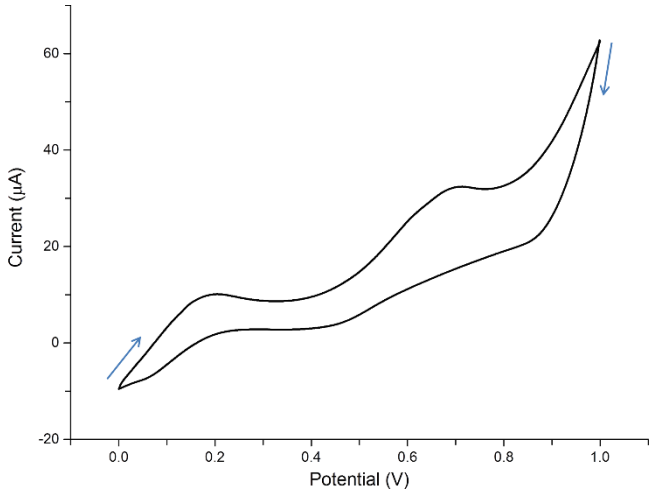

Fig. S2 The cyclic voltammogram of the electrochemical SALVI device consisting of 10 mM KI electrolyte solution, Au WE, Pt CE and Pt RE. The scan rate was 20 mV/s in the range of 0 V – 1.0 V.

Fig. S3 shows individual 3D images of key species discussed in the main text. As discussed, the adlayers (AuI^-, AuI_2^-, Au_2I^-) were transformed into the products (IO^-, IO_2^-, IO_3^-) with increased potential; and the products were converted to the adsorbed adlayers with decreased potential.

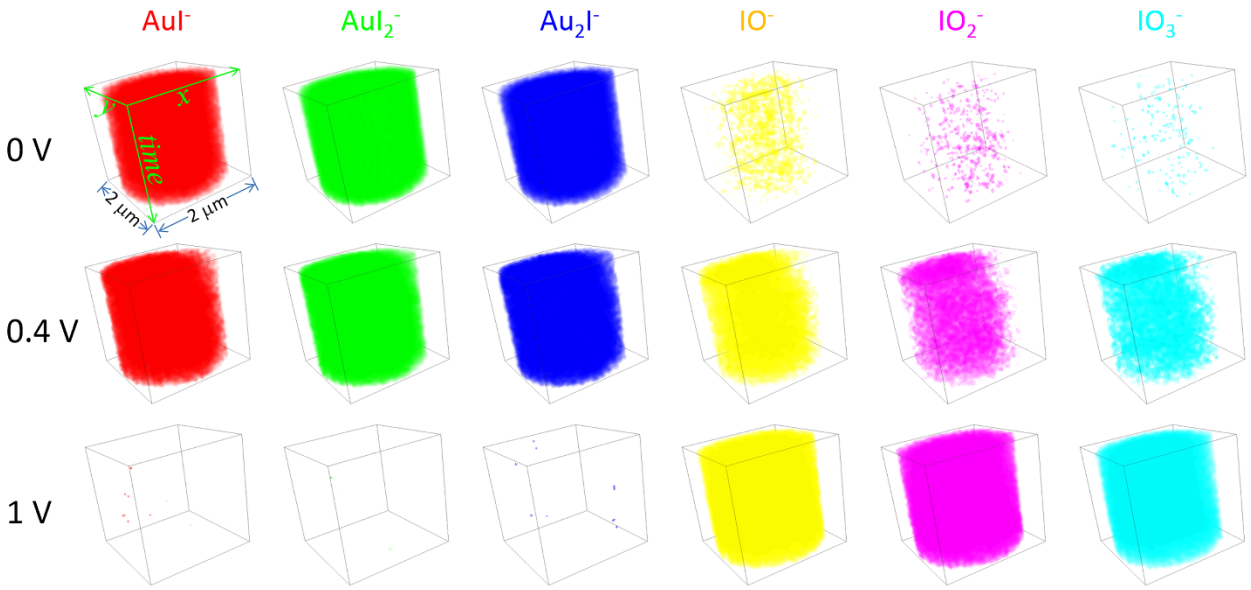

Fig. S3 3D images of key intermediates and products: AuI^-, AuI_2^-, Au_2I^-, IO^-, IO_2^-, and IO_3^- at 0 V, 0.4 V, and 1 V, respectively.

As a control, Fig. S4a and b showed the SIMS depth profiles and m/z spectra of key species (*i.e.*, AuI^-, AuI_2^-, Au_2I^-, IO^-, IO_2^-, IO_3^-, I^-, I_2^- and I_3^-) without applying any potential. Different from those in Fig. 2, all of the key species in Fig. S4 had much lower intensities except I^-. The magnitude difference ranges from 10 to 1000 times between these two conditions. This data provided supporting evidence that the key species were electrochemically generated. Another important observation from this control experiment shows that the oxidized products including IO^-, IO_2^-, and IO_3^- have similar low intensities when there is no potential applied. Compared to Fig. 2, one can see that the intensities of IO^-, IO_2^-, and IO_3^- are not the same when a potential is applied. In fact, at 0 V, IO^- has a higher count than IO_2^-; and IO_2^- has higher ion counts than IO_3^- in Fig. 2a and b. This indicates that IO^- is more easily formed in the complex chain reactions as summarized in Table 1. It is likely that IO^- is the first intermediate product before IO_2^- and IO_3^- formation. Only key species depicted in Fig. S4a are shown in Fig. S4b for clarity.

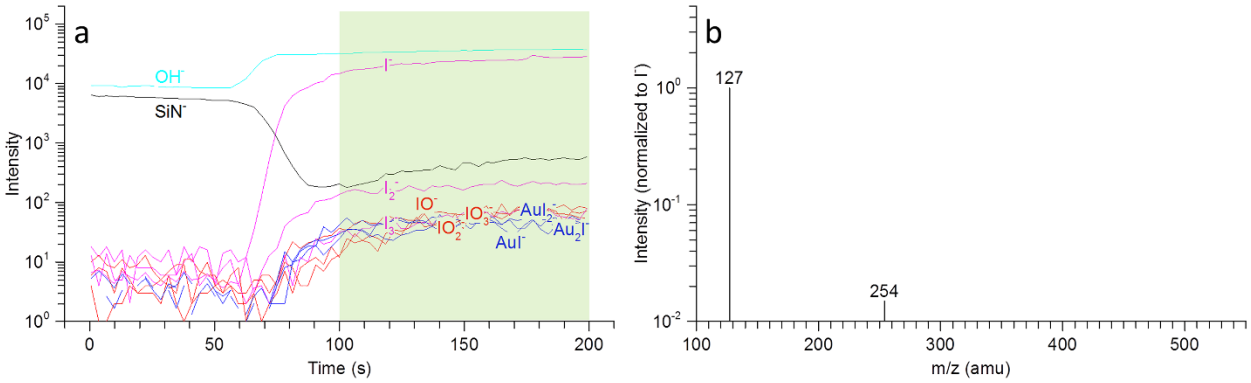

Fig. S4 (a) Depth profiles of secondary ions without applying a potential. (b) SIMS m/z spectra of key species (*e.g.*, m/z 127 I^-, m/z 254 I_2^-), data reconstructed from the shadowed area in (a).

Fig. S5a, c and e showed the normalized SIMS m/z spectra of all species reconstructed from the time series corresponding to three oxidation periods in Fig. 3, while Fig. S5b, d and f showed the normalized SIMS m/z spectra of all species reconstructed from the data during three reduction periods in Fig. 3. All six spectra were almost identical, indicating good reversibility and stability of our EC microreactor and reproducibility of the liquid SIMS analysis.

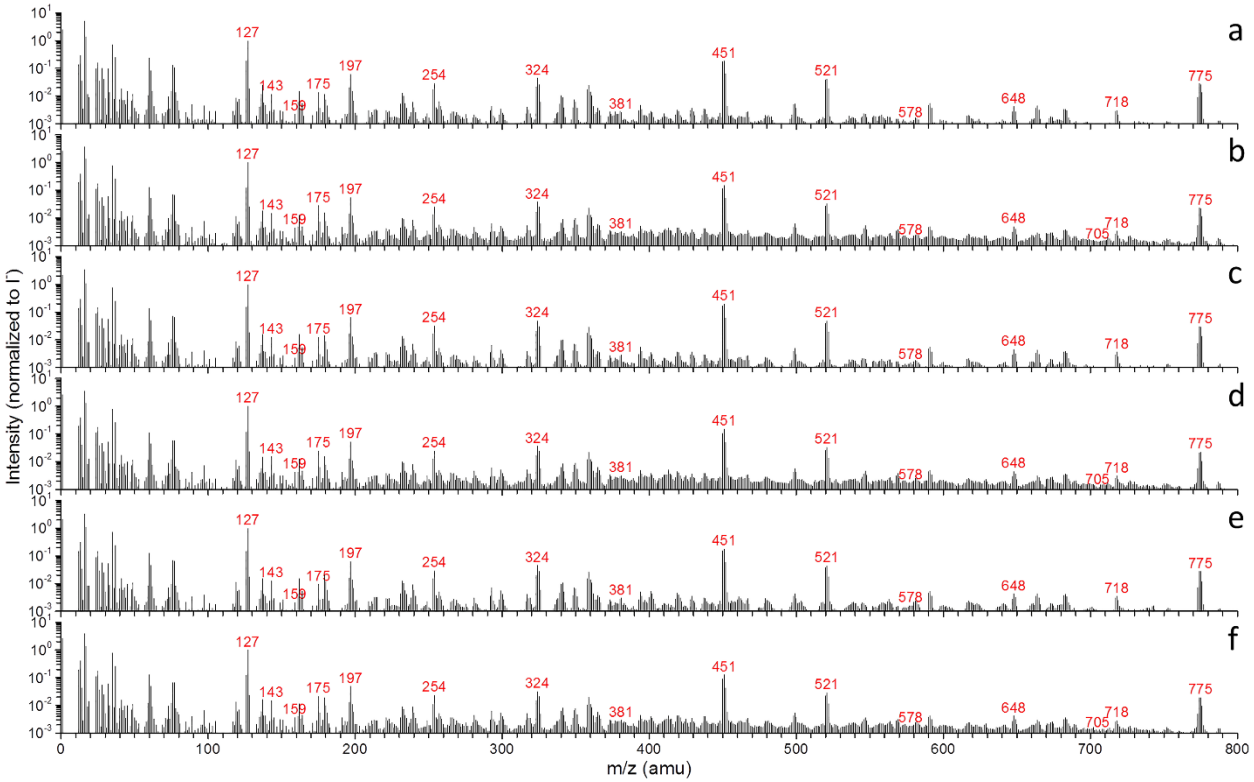

Fig. S5 SIMS m/z spectra of all species reconstructed from the data during the timeline in Fig. 3: (a) 1-50 s, (b) 51-100 s, (c) 101-150 s, (d) 151-200 s, (e) 201-250 s, and (f) 251-300 s.

SUPPLEMENTARY TABLE

Table S1 Other relevant reactions in the Au-Pt-Pt three electrode system with a dilute KI electrolyte solution.

No.	Reaction (Rxn.)	E^{θ} (V)
(S1)[4]	$Au+3I^{-}\rightleftharpoons AuI_3^{-}+2e^{-}$	
(S2)[4, 5]	$Au+4I^{-}\rightleftharpoons AuI_4^{-}+3e^{-}$	0.560
(S3)	$2Au+2I^{-}\rightleftharpoons Au_2I_2+2e^{-}$	
(S4)	$2Au+3I^{-}\rightleftharpoons Au_2I_3^{-}+2e^{-}$	
(S5)	$3Au+I^{-}\rightleftharpoons Au_3I^{2+}+3e^{-}$	
(S6)[4, 5]	$AuI_2^{-}+2I^{-}\rightleftharpoons AuI_4^{-}+2e^{-}$	0.550
(S7)[4, 5]	$I^{-}+I_2\rightleftharpoons I_3^{-}$	
(S8)[4, 5]	$2I^{-}\rightleftharpoons I_2+2e^{-}$	0.536
(S9)[4, 5]	$3I^{-}\rightleftharpoons I_3^{-}+2e^{-}$	0.536
(S10)[4, 5]	$I_2+2H_2O\rightleftharpoons 2HIO+2H^{+}+2e^{-}$	1.439
(S11)[4, 5]	$I_2+6H_2O\rightleftharpoons 2IO_3^{-}+12H^{+}+10e^{-}$	1.195
(S12)[4, 5]	$HIO+2H_2O\rightleftharpoons IO_3^{-}+5H^{+}+4e^{-}$	1.130
(S13)[6]	$2HIO\rightleftharpoons HIO_2+I^{-}+H^{+}$	

Fig. 3d showed observations of many species with lower counts. For example, AuI_3^{-} and AuI_4^{-} were electrochemically generated through Rxns. S1 and S2.[4, 5] Since the chemical compositions of $Au_2I_2^{-}$, $Au_2I_3^{-}$ and Au_3I^{-} were similar to those of AuI_2^{-}, AuI_3^{-} and AuI_4^{-}, Rxns. S3-S5 in which these species were electrochemically generated were presumed. These intermediate species formed on the electrode surface might also be transformed into redox products. Moreover, similarly to Rxn. S6,[4, 5] in which AuI_2^{-} and AuI_4^{-} were transformed between each other, all of the transient species (AuI^{-}, AuI_2^{-}, AuI_3^{-}, AuI_4^{-}, Au_2I-, $Au_2I_2^{-}$, $Au_2I_3^{-}$ and Au_3I^{-}) might be converted among themselves. On the other hand, I_2^{-} and I_3^{-} were electrochemically generated through Rxns. S7-S9,[4, 5] and consumed through reactions like Rxns. S10 and S11.[4, 5] The low intensities and complicated inter-reactions of these species have less significant effects on the potential dependence of the dynamic s-l interface. However, they were still indispensable in the integral electrochemistry.

MOVIE CAPTIONS

Movie S1 Three-dimensional illustrations of key intermediate species and products: AuI^-, AuI_2^-, Au_2I^-, IO^-, IO_2^-, and IO_3^- at 0 V, 0.4 V, and 1 V, respectively.

REFERENCES

1. L. Yang, X.-Y. Yu, Z. Zhu, M. J. Iedema and J. P. Cowin, *Lab Chip*, 2011, **11**, 2481-2484.
2. L. Yang, X.-Y. Yu, Z. Zhu, T. Thevuthasan and J. P. Cowin, *J. Vac. Sci. Technol., A*, 2011, **29**, 061101.
3. B. Liu, X.-Y. Yu, Z. Zhu, X. Hua, L. Yang and Z. Wang, *Lab Chip*, 2014, **14**, 855-859.
4. A. J. Bard, M. Stratmann, F. Scholz and C. J. Pickett, *Encyclopedia of Electrochemistry, Volume 7A, Inorganic Chemistry*, John Wiley & Sons, Weinheim, Germany, 2006.
5. W. M. Haynes, *CRC Handbook of Chemistry and Physics*, CRC Press, Boca Raton, USA, 96th edn., 2015.
6. I. Lengyel, J. Li, K. Kustin and I. R. Epstein, *J. Am. Chem. Soc.*, 1996, **118**, 3708-3719.